

Estimating Fracture Toughness Using Tension or Ball Indentation Tests and a Modified Critical Strain Model

F. M. Haggag and R. K. Nanstad
Metals and Ceramics Division
Oak Ridge National Laboratory
Oak Ridge, Tennessee 37831

ABSTRACT

A simple technique is described for estimating the fracture toughness by coupling the measured flow properties (either from a uniaxial tensile test or from a new automated ball indentation test) with a modified but empirically correlated critical fracture strain model. This technique is currently limited to ductile fracture applications.

The modified model was used in combination with either tensile or ball indentation data to estimate fracture toughness of A515 grade 70 carbon steel and A533 grade B class 1 pressure vessel steel, respectively. The difference between fracture toughness predictions and measured values, using a computerized single-specimen unloading compliance technique in accordance with ASTM E-813, was less than 11%.

INTRODUCTION

The measurement of fracture toughness of metallic materials according to ASTM standard test methods (E-399 or E-813) is expensive as well as material and time consuming. Although these measurements are essential for proper fracture mechanics evaluation, still there is a considerable interest in approximate, rapid, and relatively less expensive fracture toughness test methods. These methods, though limited in range of applicability, are particularly important in the early stages of product or new alloy development.

The critical fracture strain model for ductile fracture prediction can be expressed in the form (1, 2):

$$K_{J_{IC}} = \text{Constant} (\epsilon_f^* \cdot l_0^* \cdot E \cdot \sigma_y)^{0.5} \quad (1)$$

where $K_{J_{IC}}$ is the fracture toughness calculated from J_{IC} , ϵ_f^* is the critical fracture strain, l_0^* is the characteristic distance ahead of the crack tip over which the strain must exceed ϵ_f^* , E is the elastic modulus, and σ_y is the yield

strength. The modification (3) of this model involved: (1) the use of measured uniform strain from tensile tests or the strain-hardening exponent from automated ball indentation (ABI) tests instead of the critical fracture strain value required in the original model, and (2) the assumption of an empirically calibrated value for the characteristic distance, l_0^* , for each class of material. The modified model was used to estimate fracture toughness of two steel materials, A515 grade 70 (using smooth tensile specimens, Ref. 4) and A533 grade B class 1 (using ABI test results obtained in this work). The determination of the critical fracture strain, ϵ_f^* , requires testing of several circumferentially notched round tensile specimens each having a different value of its notch root radius. Values of the critical fracture strain, (ϵ_f^* , were not determined for the two steel materials in this work. The ABI test technique used in this work provides an alternative method to determine the yield strength, σ_y , and the strain-hardening exponent, n , (for most metals exhibiting a power law behavior one can mathematically prove that the strain-hardening exponent, n , is equal to the uniform ductility, ϵ_u) in an almost nondestructive manner which will be more favorable over tensile testing for field applications and when limited materials are available. In accordance with ASTM Standard E-646-78, the uniform plastic elongation part of the uniaxial tensile true-stress, σ_t , versus true-plastic-strain, ϵ_p , curve of many metallic materials can be mathematically represented by a power curve of the form: $\sigma_t = K \epsilon_p^n$, where K is the strength coefficient and n is the strain-hardening exponent. Details of the ABI test technique as well as a comparison between ABI and tensile test results (particularly σ_y and n values) on both unirradiated and irradiated pressure vessel steels are given in Ref. 5.

The characteristic distance, l_0^* , for ductile fracture is usually a multiple of the interparticle spacing and currently it should be regarded as essentially an empirically obtained quantity. Although this dimension is presumably of relevance to the microstructural aspects of fracture

initiation it is plausibly related to the yield strength, strain-hardening exponent (a measure of work-hardening), and the strength coefficient of the test material. However, more research is needed to better quantify and define ϵ_o^* to enable use of this method of estimating fracture toughness for applications where this characteristic distance is expected to change (e.g. due to radiation embrittlement).

RESULTS AND DISCUSSION

Estimation of Fracture Toughness from Tensile Data:

The modified critical strain model can now be written as:

$$K_{J_{ic}} = \text{Constant} (\epsilon_u \cdot \epsilon_o^* \cdot E \cdot \sigma_y)^{0.5}, \quad (2)$$

where ϵ_u is the uniform strain (value of strain corresponding to maximum load). Equation (2) was used successfully to estimate fracture toughness from tensile test results (4). In that previous study, three large flat tensile specimens (1.63 cm thick, 7.7 cm wide, and 15.2 cm gage section) were machined from A515 grade 70 steel plate (61 x 61 cm x 1.63 cm thick) with their axes aligned with the transverse direction of the plate. These specimens were pulled at room temperature until their gage sections reached 4, 8, and 12% strains, respectively. After straining, smaller round tensile specimens and three-point bend specimens were machined from the prior-strained reduced sections. The three-point bend specimens were then fatigue precracked. The small round tensile specimens were tested according to ASTM Standard E-8-82 and the precracked three-point bend specimens were tested using a computerized single-specimen unloading compliance technique to measure J_{ic} according to ASTM E-813-81. (Broken three-point bend specimens, tested earlier in Ref. 4, were not available for ABI testing.) The fracture toughness was then calculated from the J_{ic} values using the equation:

$$K_{J_{ic}}^2 = J_{ic} \cdot E. \quad (3)$$

Since the critical fracture strain, ϵ_f^* , values were not determined experimentally, uniform strain values were used in the calculations (3, 6). Although such a substitution has no theoretical basis, it was considered reasonable since the critical fracture strain is often proportional to the uniform strain for a smooth tensile specimen (6). The proportionality constant would thus be included in the constant coefficient of Eq. (2). The value of 3.00 for this constant is good for steels whether in the irradiated (3) or deformed (4) condition; however, this value might be different for other classes of materials such as titanium or aluminum alloys, etc., and further research is needed to determine the appropriate value of this constant via empirical correlation. The values of the elastic modulus at room temperature and at 73 °C were estimated as 206 and 203 GPa, respectively. The critical characteristic distance, ϵ_o^* , is a multiple of the planar inclusion spacing (spacing between major voids on a fractured surface) and is obtained empirically. Scanning electron microscopy examination of the A515 steel material showed that the average spacing between major voids on the material fracture surface for all prior strains

was roughly 250 μm (4). Hence, a characteristic distance equivalent to the average spacing between major voids (250 μm) was assumed for all specimens (similar to Ritchie's work (2) on A302 grade B pressure vessel steel). It was assumed that this characteristic distance did not change due to deformation (or prior strain) of the A515 steel specimens; however, this might not be true for irradiated materials. Ritchie (2) stated that the characteristic distance for ductile fracture might be a function of both the microstructure (i.e., the inter-inclusion spacing) and of the average number of voids which coalesce with the crack tip at fracture initiation (slow crack growth). Hence, it is not certain that the same number of voids will be involved at fracture initiation in irradiated steel because the reduced strain hardening capacity of the irradiated material will result in earlier coalescence by plastic shear localization of major voids. The difference between predicted and measured toughness values for the A515 steel specimens was less than 11% (see Table 1). The largest error of the material tested at room temperature (0 prior strain), as shown in Table 1, is believed to be primarily due to experimental scatter.

Estimation of Fracture Toughness from ABI Data:

For estimating fracture toughness in certain applications, ABI testing might replace tensile testing because it is simpler, faster, nondestructive, and could be performed in-situ (using a field apparatus) to evaluate deformed components, and aged and embrittled structural components (provided that characteristic distance values are available). Furthermore, the ABI technique uses a very small volume of test material. Hence, it could prove valuable in new alloy development and when limited amounts of material are available. Other applications might include weld characterization and qualification, testing of near-net-shape manufactured components, and residual life assessment.

The ABI test is based on multiple indentations (at the same penetration location) of a polished metallic surface by a spherical indenter. This is accomplished by cyclic loading and unloading of the indenter into the test material where the load is increased in the successive loading cycles. The applied loads and associated displacements (depth of penetration of the indenter into the test specimen) are measured during both loading and unloading using a load cell and a linear variable differential transducer (LVDT). The test set-up of the current work used a 1.59-mm diameter ball indenter and a spring loaded LVDT which were mounted to the load cell of an MTS hydraulic testing machine. A photograph of the ball indenter and the LVDT are shown in Fig.1. An in-house data acquisition and control system and a Hewlett-Packard computer were used for automated testing as well as acquiring and processing test data. The load-displacement data were used to determine the yield strength and produce the ABI-derived true-stress/true-plastic-strain curve. The ABI analyses are based primarily on elasticity and plasticity theories and some empirically calibrated correlations as described in Refs. 5 and 7.

The ABI tests were conducted on the side surfaces far from the fracture planes of 25.4-mm-thick compact specimens (1TCS) of A533 grade B class 1 pressure vessel steel. These specimens were tested previously according to ASTM E-813-81 and the fracture toughness values were reported in Ref. 8. The ABI load-displacement curve of one of these specimens is shown in Fig. 2. The yield strength was calculated from the measured values of the load (P) and the chordal indentation diameter (d_c) during load application for the indentation cycles of the entire curve of Fig. 2. This is illustrated in Fig. 3 where D is the diameter of the ball indenter. Details of the ABI test procedures are given in Ref. 5. The strain-hardening exponent, n , was determined according to the procedure of ASTM E-646-78 as the slope of the true-stress/true-plastic-strain curve when plotted on a log-log scale as shown in Fig. 4. For metallic materials for which plastic-flow behavior obeys a power law, the strain-hardening exponent should be equal to the uniform elongation. Hence, ABI-derived values of n were used instead of ϵ_u in Eq. (2) to estimate fracture toughness. The elastic modulus was assumed to be 206 GPa for both materials. Fractographic examination of the fracture surfaces of these A533 grade B class 1 steel specimens showed that the average spacing between major voids was roughly 50 μm (consistent with previous studies (2)). Using a multiplication factor of 7, the characteristic distance was assumed to be 350 μm as reported earlier for A533 grade B class 1 steel by Ritchie et al (2). Table 2 shows a comparison between ABI-estimated and measured fracture toughness values for these A533 grade B class 1 steel specimens. The difference between estimated and measured toughness values was less than 11%. Additional ABI tests were conducted on these two broken halves of 1TCS specimens and the results were very similar to those reported in Table 2 which represented the upper and lower bounds of all ABI tests.

Good agreement between ABI-derived and tensile flow properties has been demonstrated for unirradiated and irradiated A212 grade B pressure vessel steel specimens (5). In Ref. 5 it is shown that the difference between the average values of yield strength measured by ABI and tensile tests was less than 2%. Furthermore, the ABI-measured flow properties showed an excellent agreement with those measured from a uniaxial tensile test, as shown in Fig. 5, for an irradiated A212 grade B pressure vessel steel. Values of the strain-hardening exponent, n , measured for these two irradiated specimens of Fig. 5 using ABI and uniaxial tensile tests are 0.192 and 0.195, respectively.

CONCLUSIONS

A simple technique was described for estimating the fracture toughness by coupling the measured flow properties (either from a uniaxial tensile test or from a new automated ball indentation test) with a modified but empirically correlated critical fracture strain model. This technique predicted fracture toughness values that differed by less than 11% from measured values for both A515 grade 70 and A533 grade B class 1 steels. Although the

ABI technique is limited to near-surface materials evaluation, its localized and nondestructive features make it valuable in determining local material property variations.

Currently, the technique is limited to ductile fracture applications. The empirical value for the characteristic distance should be used with caution since severe heat treatment or neutron irradiation conditions could alter it. The empirical determination of the characteristic distance is a limiting factor for the applicability of the methods discussed in this paper for estimating fracture toughness. Additional research is needed to modify and improve the model where such an empirical determination will be no longer required possibly by incorporating the microstructural effects into the macroscopic behavior (e.g., flow properties) of the test material.

ACKNOWLEDGMENT

This work was partially supported by the office of Nuclear Regulatory Research, Division of Engineering, U. S. Nuclear Regulatory Commission under Interagency Agreement DOE 1886-8011-9B with the U.S. Department of Energy under contract DE-AC05-84OR21400 with Martin Marietta Energy Systems, Inc.

REFERENCES

1. Pandey, R. K., and Banerjee, S., "Strain Induced Fracture in Low Strength Steels," *Eng. Fract. Mech.*/Vol. 10 (1978), pp. 817-29.
2. Ritchie, R. O., Server, W. L., and Waullaert, R. A., "Critical Fracture Stress and Fracture Strain Models for Prediction of Lower and Upper Shelf Toughness in Nuclear Pressure Vessel Steels," *Met. Trans. A*, Vol. 10A (1979) pp. 1557-70.
3. Haggag, F. M., Reuter, W. G., and Server, W. L., "Recovery of Fracture Toughness of Irradiated Type 347 Stainless Steel Due to Thermal Stress Relief: Metallographic and Fractographic Studies," *Proceedings of the 2nd International Symposium on Environmental Degradation of Materials in Nuclear Power Systems-Water Reactors*, Monterey, California, September 9-12, 1985, (1986) pp. 509-14.
4. Haggag, F. M., Server, W. L., Lucas, G. E., Odette, G. R., and Sheckherd, J. W., "The Use of Miniaturized Tests to Predict Flow Properties and Estimate Fracture Toughness in Deformed Steel Plates," *Proceedings of the ASM International Conference and Exposition on Fatigue, Corrosion Cracking, Fracture Mechanics and Failure Analysis*, Volume: *The Mechanism of Fracture*, December 2-6, 1985 (1986), pp. 399-406.

5. Haggag, F. M., Nanstad, R. K., and Braski, D. N., "Structural Integrity Evaluation Based on an Innovative Field Indentation Microprobe," to be presented at the ASME Pressure Vessel and Piping Conference, Honolulu, Hawaii, July 23-27, 1989.

6. Pavinich, W. A., "The Effect of Neutron Fluence and Temperature on the Fracture Toughness and Tensile Properties for a Linde 80 Submerged Arc Weld," Proceedings of the 2nd International Symposium on Environmental Degradation of Materials in Nuclear Power Systems-Water Reactors, Monterey, California, September 9-12, 1985, (1986) pp. 485-95.

7. Haggag, F. M., "Field Indentation Microprobe for Structural Integrity Evaluation", U. S. Patent pending, 1988.

8. Naus, D. J., Nanstad, R. K., Bass, B. R., Merkle, J. G., Pugh, C. E., Corwin, W. R., and Robinson, G. C., "Crack-Arrest Behavior in SEN Wide Plates of Quenched and Tempered A 533 Grade B Steel Tested Under Nonisothermal Conditions," NUREG/CR-4930, ORNL-6388, Oak Ridge National Laboratory, Oak Ridge, Tennessee, August 1987, p. 31.

Table 1. Comparison of Predicted (Using Tensile Data) and Measured Fracture Toughness Values for A515 grade 70 Steel

Test Temp. (C)	Prior Strain (%)	Tensile Test Data		K _{JIC} (Mpa · m ^{0.5})		
		Yield Strength (Mpa)	Uniform Elong. (%)	A (Measured)	B (Tensile-Predicted)	$\frac{B-A}{A}$ (%)
23	0	314	19.4	152	168	+10.5
23	4	546	10.8	167	156	-6.6
23	8	635	7.6	149	150	+0.7
23	12	685	4.4	126	118	-6.3
73	0	297	18.1	154	157	+1.9

Table 2. Comparison of Predicted (Using ABI Data) and Measured Fracture Toughness Values for A533 grade B Class 1 Steel Tested at Room Temperature

Specimen Number	ABI Test Data		K _{JIC} (Mpa · m ^{0.5})		
	Yield Strength (Mpa)	n	A (Measured)	B (ABI-Predicted)	$\frac{B-A}{A}$ (%)
K52C	400	0.187	198.5	220.3	+11.0
K53A	407	0.173	234.1	213.8	-8.7
		Average:	216.3	217.1	+0.4

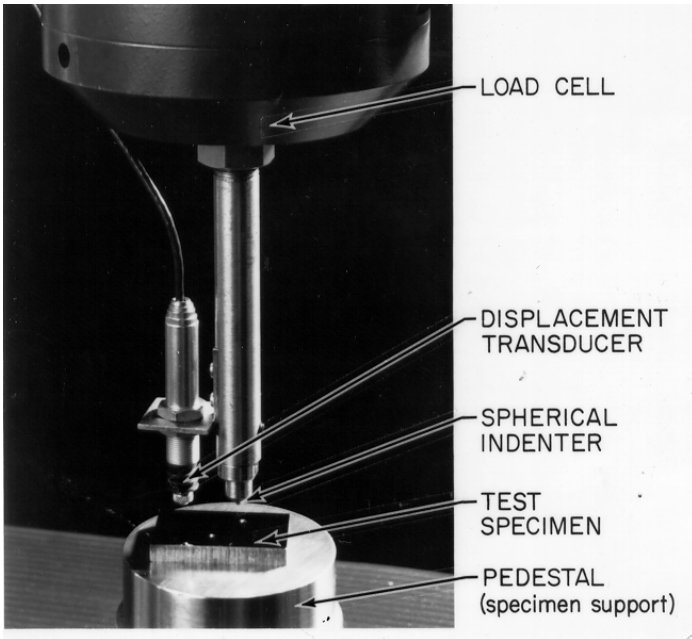


Fig. 1 Ball indenter and spring-loaded LVDT mounted to the load cell of a hydraulic testing machine (not shown in figure).

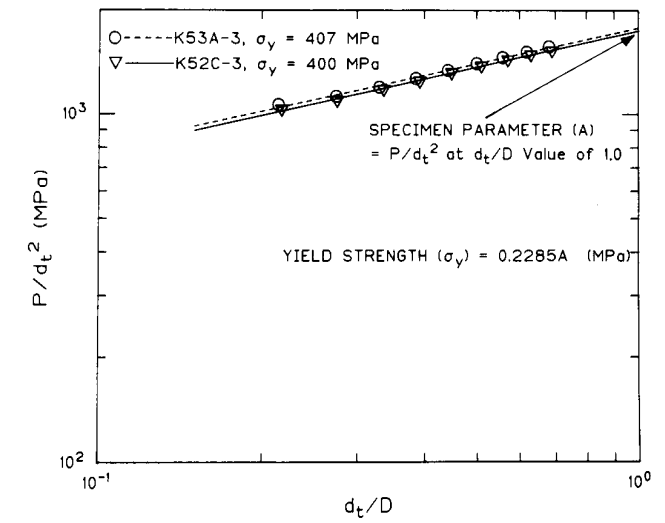


Fig. 3 Yield strength results calculated from the entire ABI load-displaced curve for two tests on broken halves of A533B steel fracture toughness specimens.

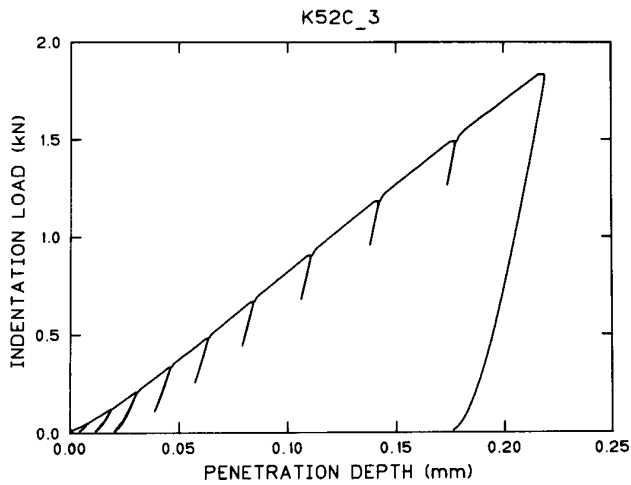


Fig. 2 Sample of ABI test results (load versus displacement using a 1.59-mm diameter ball indenter) on A533B pressure vessel steel.

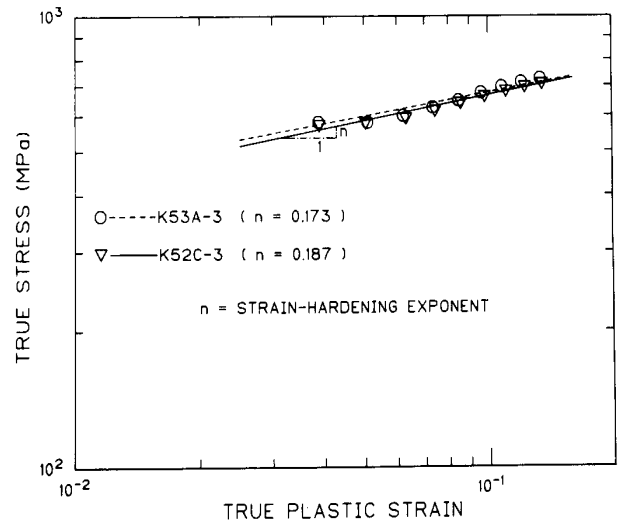


Fig. 4 Flow properties measured from ABI tests conducted on two broken halves of A533B steel fracture toughness specimens. (Note that each curve is entirely obtained from multiple indentations at a single penetration location.)

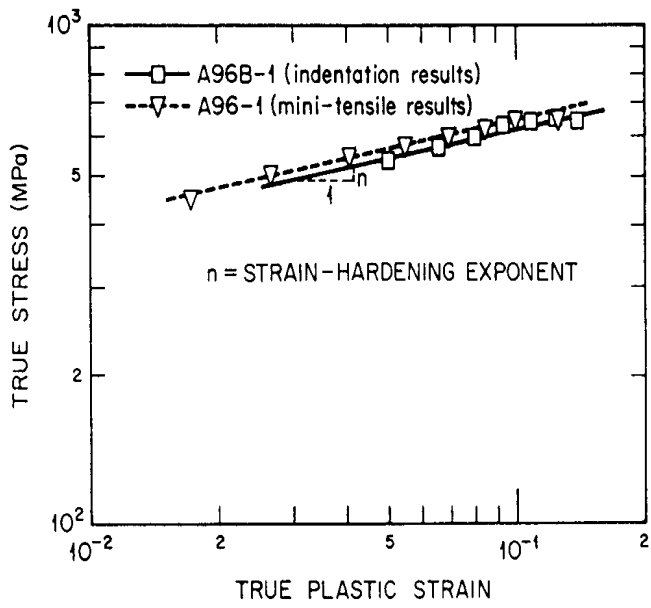


Fig. 5 Comparison between flow properties (true-stress/true-plastic-strain curve) measured from ABI and uniaxial tensile tests on irradiated A212B pressure vessel steel.